Left-Ventricular Co-Abundance Protein Modules Distinguishing Decompensated Heart Failure Across Ischemic, Dilated, and Hypertrophic Etiologies

A Reproducible, Cross-Etiology Proteomic Re-Analysis of ProteomeXchange/PRIDE `PXD008934` (Revision 3)

Technical Report

Discovery framework: co-abundance modules → age/sex-adjusted empirical-Bayes contrasts → cross-etiology heterogeneity → stability-based *Validate / Replicate-First / Deprioritize* triage

Scope statement. All effect sizes reported here are **total protein-abundance** $\log_2$ fold-changes derived from label-free MaxQuant (LFQ) intensities aggregated at the protein-group level. **No post-translational modification (PTM) state is measured or inferred** at any point in this analysis or in the downstream validation plan.

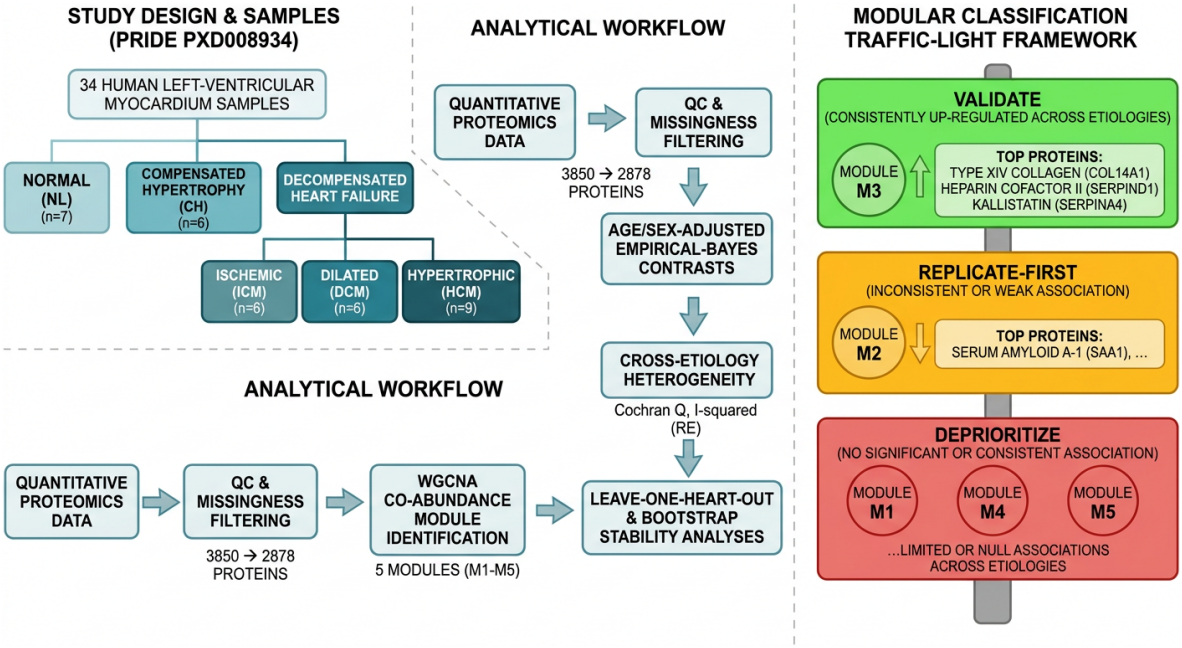

Data source: EBI PRIDE Archive, accession `PXD008934` (revision 3). Analysis date: July 2026.

Contents

1 Executive Summary

Decompensated heart failure (DHF) represents the terminal, clinically catastrophic phase of a wide range of cardiac diseases, yet the molecular signatures that mark the transition out of a stable, compensated state — and that are shared across otherwise dissimilar etiologies — remain incompletely defined. This report re-analyzes the human left-ventricular (LV) proteome from ProteomeXchange/PRIDE accession `PXD008934` (Chen *et al.*, *Nature Medicine* 2018) [1], comprising label-free quantitative (LFQ) mass-spectrometry measurements of 34 LV myocardial specimens spanning normal donor hearts (NL, $n = 7$), compensated hypertrophy (CH, $n = 6$), and decompensated failing hearts of ischemic (ICM, $n = 6$), dilated (DCM, $n = 6$), and hypertrophic (HCM, $n = 9$) origin. Our objective was not to re-derive the original study's microtubule findings, but to ask an orthogonal, network-level question: *which co-abundance protein modules separate DHF from both non-failing references, remain directionally consistent across the three etiologies, and are statistically stable enough to warrant experimental validation?*

Beginning from the processed MaxQuant `proteinGroups.txt` matrix, we reproduced a stringent contaminant/decoy and missingness filtering cascade (3,850 → 2,878 protein groups), performed down-shifted imputation of low-abundance missing values, and mapped each specimen to a precise clinical phenotype using patient-level metadata. We then constructed a weighted, signed co-abundance network (WGCNA-style; soft-threshold $\beta = 15$), resolving five robust modules (M1–M5). For every protein and every module eigengene we fit age- and sex-adjusted linear models with limma-style empirical-Bayes (EB) variance moderation, contrasting pooled DHF against NL and against CH. Cross-etiology heterogeneity was quantified with fixed-effect Cochran's Q and I^2 statistics computed across ICM/DCM/HCM against both references, and module partition stability was assessed by 34 leave-one-heart-out (LOHO) re-clusterings and 100 bootstrap resamplings.

Headline finding: Module M3 is the single Validate-tier candidate

Module **M3** (565 proteins) is coordinately **up-regulated in DHF** relative to *both* non-failing references, is **directionally homogeneous across all three etiologies** ($I^2 = 0\%$; Cochran's Q $p = 0.43$ vs NL, $p = 0.74$ vs CH), reaches module-level significance in both main contrasts (FDR < 0.001), and possesses a **reproducible eigengene** under leave-one-heart-out resampling (mean $|r| = 0.82$). It is therefore the sole module meeting the highest-priority **"Validate"** criteria. At the protein level, **31 proteins** qualify as Validate and **44** as Replicate-First; **18 of the top-20** ranked Validate candidates belong to M3.

The leading, etiology-robust M3 candidates — ranked by the *minimum* absolute fold-change observed across all six etiology-specific contrasts, i.e., their weakest guaranteed effect — are dominated by extracellular-matrix and plasma/coagulation proteins: *COL14A1* (collagen XIV), *SERPIND1* (heparin cofactor II), *SERPINA4* (kallistatin), *HRG* (histidine-rich glycoprotein), *AHSG* (fetuin-A), *CLEC3B* (tetranectin), *PLG* (plasminogen), and the cardiomyocyte intermediate-filament protein *SYNM* (synemin). Two further proteins reach protein-level Validate status through the high eigengene reproducibility of their host modules: *SAA1* (serum amyloid A, consistently *down* in M2) and *FLOT1* (flotillin-1, up in M1). Modules M2 (highly reproducible eigengene but etiology-divergent, $I^2 \approx 82\%$) and M1/M4/M5 are triaged as Replicate-First and Deprioritize, respectively.

Two caveats materially shape our recommendation. First, a substantial fraction of the top M3 candidates are abundant plasma, acute-phase, and erythrocyte proteins whose coordinated rise in decompensated myocardium may partly reflect **intramyocardial blood retention, congestion, and edema** rather than resident-cell expression; the validation plan therefore embeds perfusion and hemoglobin-covariate controls and prioritizes functional follow-up on candidates with plausible resident-cell biology (*COL14A1*, *SYNM*, *FLOT1*). Second, *CRP* (C-reactive protein), although biologically compelling and statistically significant, is **quantitatively deprioritized** because its cross-etiology magnitude is heterogeneous ($I^2 \approx 58\%$); it is retained only as an inflammatory

reference marker. We close with a concrete, tiered orthogonal validation program (targeted PRM/SRM mass spectrometry, antibody-based confirmation, and functional interrogation) built strictly around total protein abundance.

2 Introduction

2.1 The clinical and biological problem of decompensation

Heart failure remains one of the largest contributors to global cardiovascular morbidity and mortality, affecting an estimated 64 million people worldwide and consuming a disproportionate share of healthcare resources [2, 3]. A defining feature of its natural history is that the myocardium can sustain considerable hemodynamic stress for years within a *compensated* state — maintaining cardiac output through hypertrophy, altered calcium handling, and metabolic and matrix remodeling — before undergoing a comparatively abrupt transition into *decompensation*, characterized by pump failure, congestion, and a steep rise in mortality [4, 5]. Understanding the molecular determinants of this transition is of central therapeutic importance: interventions that stabilize a compensated phenotype, or that reverse early decompensation, would have far greater clinical impact than treatments applied at the end stage.

The compensated-to-decompensated transition is not a single molecular event but a convergence of processes. Chronic pressure or volume overload drives cardiomyocyte hypertrophy and re-expression of a fetal gene program; sustained stress precipitates energetic and mitochondrial insufficiency that can precede overt systolic failure [6]; and a maladaptive inflammatory and fibrotic response progressively stiffens and disorganizes the extracellular matrix (ECM) [7]. Whether these programs converge on a shared, measurable protein signature — one that is present regardless of the initiating insult — is a question that network-level proteomics is well positioned to address.

2.2 Etiologic heterogeneity: ischemic, dilated, and hypertrophic disease

The three etiologies represented in `PXD008934` arise from mechanistically distinct origins. **Ischemic cardiomyopathy (ICM)** results from coronary obstruction and infarction, producing regional myocyte loss, replacement fibrosis, and adverse remodeling of surviving myocardium [8]. **Dilated cardiomyopathy (DCM)** is characterized by ventricular chamber enlargement and systolic dysfunction, frequently with a genetic or inflammatory basis and diffuse interstitial fibrosis. **Hypertrophic cardiomyopathy (HCM)**, most commonly caused by sarcomeric protein mutations, produces asymmetric hypertrophy, myofibrillar disarray, and both preserved- and reduced-ejection-fraction failing phenotypes (HCMpEF and HCMrEF) [9]. A protein signature that is directionally consistent across such divergent starting points is, by construction, more likely to reflect the *shared physiology of decompensation* than the idiosyncrasies of any single disease — and is correspondingly more attractive as a generalizable biomarker or therapeutic target. Conversely, signatures that diverge in sign or magnitude across etiologies, however statistically striking within one disease, are poor candidates for pan-etiology translation and must be treated with caution.

2.3 Proteomics and the modular view of myocardial remodeling

Mass-spectrometry proteomics provides a direct, near-comprehensive readout of the myocardial protein complement, and region- and cell-type-resolved maps of the human heart have established that cardiac tissue possesses a highly structured, spatially organized proteome [10]. Rather than treating each of several thousand proteins as an independent test — an approach that is both statistically underpowered in small human cohorts and biologically artificial — weighted co-abundance network analysis (WGCNA) groups proteins into *modules* of coordinated behavior and summarizes each module by an eigengene [11, 12]. Modules concentrate biological signal, reduce the multiple-testing burden, and, crucially for the present question, provide a natural unit at which to assess reproducibility and cross-condition consistency. Pairing modules with

empirical-Bayes moderated linear models [13, 14] yields stable inference even at the modest sample sizes typical of human myocardial studies.

2.4 Dataset and objectives

The `PXD008934` dataset was generated by Chen *et al.* to study detyrosinated-microtubule mechanics in human heart failure [1]; here we repurpose its processed LFQ matrix for an entirely distinct, network-level question and apply a triage framework oriented toward experimental prioritization. Working from revision 3 of the archived record, our specific objectives were to: (i) faithfully reproduce contaminant/decoy and missingness filtering on the processed LFQ data; (ii) identify LV co-abundance modules that separate DHF from NL and from CH; (iii) fit age- and sex-adjusted empirical-Bayes contrasts at both the protein and module level; (iv) quantify cross-etiology heterogeneity and directional consistency using meta-analytic statistics (Q, I^2); (v) evaluate module stability by leave-one-heart-out and bootstrap resampling; and (vi) deliver a short, ranked list of modules and proteins together with a defensible *Validate / Replicate-First / Deprioritize* recommendation and a concrete orthogonal validation plan. Throughout, we deliberately restrict all inference to total protein abundance and make no claim about post-translational modification state.

3 Methodology

3.1 Data acquisition and curation

The processed proteomic data for accession `PXD008934` were retrieved programmatically from the EBI PRIDE Archive via the PRIDE REST API and its HTTPS file mirror [15, 16]. The quantitative core of the dataset — the MaxQuant [17] `proteinGroups.txt` matrix (3,850 protein groups × 341 columns, including 34 `LFQ intensity` sample columns), together with the supporting `peptides.txt`, `summary.txt`, and `parameters.txt` tables — resides inside a 1.9 GB MaxQuant archive. To avoid transferring the entire archive, HTTP byte-range requests were used to extract only these four tables (∼90 MB). Raw spectra and search intermediates were intentionally not downloaded, as they are unnecessary for re-analysis of the processed matrix. Sample-level clinical annotation was obtained from the archived SDRF file and the patient-details table, and all key tables were loaded and dimension-verified before analysis. The full provenance and integrity report is retained with the analysis outputs.

3.2 Clinical phenotype mapping

Because the SDRF disease field is only partially granular (several hearts carry a generic "cardiac hypertrophy" label), precise etiology was taken from the patient-details table and joined to each LFQ column through the MaxQuant raw-file identifier. This step resolved a known identifier mismatch in which one specimen (nominal individual `S1609`) is measured in the column `LFQ intensity S1605` (phenotype DHF–DCM). The resulting phenotype assignment yields five analysis groups — NL ($n = 7$), CH ($n = 6$), DHF–ICM ($n = 6$), DHF–DCM ($n = 6$), and DHF–HCM ($n = 9$, comprising 5 HCMrEF and 4 HCMpEF) — with 23 male and 11 female donors. Age, sex, heart weight, body-mass index, and left-ventricular ejection fraction were extracted as covariates for downstream modeling.

3.3 Quality control and missingness filtering

Filtering of the `proteinGroups.txt` matrix reproduced a standard MaxQuant/Perseus-style cascade [18]. Beginning from 3,850 protein groups, we removed 44 reverse (decoy) hits, 37 potential contaminants, and 67 groups identified only by modification site, leaving 3,713 groups. The 34 LFQ columns were $\log_2$-transformed (zero/absent values set to missing). A group-wise missingness

filter then required at least 70% valid (non-missing) values in at least one of the five phenotype groups (NL/CH/ICM/DCM/HCM), retaining **2,878 protein groups**. Within this filtered matrix, 10,751 of 97,852 values (10.99%) were missing.

3.4 Imputation

Missing values were imputed using a down-shifted normal (Perseus-style) model applied column-wise: for each sample, imputed values were drawn from $\mathcal{N}(\mu - 1.8\sigma,\ (0.3\sigma)^2)$, where μ and σ are the mean and standard deviation of the observed values in that column. This models values missing-not-at-random due to low abundance below the detection limit — the dominant missingness mechanism in LFQ proteomics — and is the field-standard choice, although downstream sensitivity to imputation is acknowledged as a general limitation [19]. All 10,751 missing values were imputed (seed fixed for reproducibility); no missing values remained. Per-sample $\log_2$ LFQ distributions were confirmed to be comparable before and after imputation.

3.5 Co-abundance module identification

A signed, weighted co-abundance network was built over the 2,878 imputed proteins following the WGCNA framework [11, 12]. Pairwise Pearson correlations across the 34 samples were transformed into a signed similarity $s_{ij} = 0.5\,(1 + r_{ij})$ and raised to a soft-thresholding power β to form the adjacency $A_{ij} = s_{ij}^{\beta}$. A power sweep over $\beta \in \{4, \ldots, 20\}$ selected the smallest power achieving a signed scale-free topology fit of $R^2 \geq 0.8$, namely $\beta = 15$ (mean connectivity $\langle k \rangle = 4.78$). The topological overlap matrix (TOM) was computed from the adjacency, and average-linkage hierarchical clustering was applied to the dissimilarity $1 - \mathrm{TOM}$. The cut height was searched to yield modules containing at least 20 proteins each, producing five modules (M1–M5) plus an unassigned "grey" set (M0). Each module eigengene (ME) was defined as the first principal component of the module's z-scored expression, sign-aligned so that a positive ME corresponds to higher mean abundance.

3.6 Age- and sex-adjusted empirical-Bayes contrasts

For every protein and every module eigengene, an ordinary least-squares model of the form

$$\text{Expression} \;=\; \beta_0 + \beta_1\,\text{Group} + \beta_2\,\text{Age} + \beta_3\,\text{Sex} + \varepsilon$$

was fit (Sex encoded male = 1, female = 0), where the Group coefficient β_1 is the $\log_2$ fold-change of interest. Two primary contrasts were evaluated: pooled DHF (ICM+DCM+HCM, $n = 21$) versus NL ($n = 7$), and pooled DHF versus CH ($n = 6$). Empirical-Bayes moderation followed the limma formulation [13, 14]: residual variances were fit to a scaled F-distribution to obtain a prior degrees-of-freedom d_0 and scale s_0^2; the moderated variance $\tilde{s}^2 = (d_0 s_0^2 + d\,s^2)/(d_0 + d)$ was used to form moderated t-statistics on $d + d_0$ degrees of freedom; and p-values were adjusted by the Benjamini–Hochberg procedure to control the false-discovery rate (FDR) [20]. Protein-level analyses used EB-moderated variances throughout; module-eigengene analyses ($k = 5$ features) used ordinary OLS standard errors, for which EB shrinkage is unreliable.

3.7 Cross-etiology heterogeneity and directional consistency

To test whether effects generalize across etiologies, age/sex-adjusted linear models were additionally fit for each individual etiology (ICM, DCM, HCM) against each non-failing reference (NL and CH separately), yielding six etiology-specific contrasts per feature. Fixed-effect Cochran's Q and the I^2 inconsistency statistic [21–23] were computed across the three etiologies (inverse-variance weights $w_i = 1/\mathrm{SE}_i^2$), separately for the vs-NL and vs-CH comparisons, with a χ^2 (df = 2) p-value for Q. A feature was labeled **directionally consistent** when the sign of its $\log_2$ fold-change

agreed across all three etiologies for *both* references and heterogeneity was low ($I^2 < 50\%$ or Q $p > 0.05$) for both references.

3.8 Module stability: leave-one-heart-out and bootstrap

Two complementary resampling schemes probed the stability of the module partition, using an identical clustering pipeline (verified to reproduce the primary solution with adjusted Rand index, ARI = 1.0). In **leave-one-heart-out (LOHO)** analysis, each of the 34 samples was removed in turn and the remaining 33 re-clustered; new modules were matched to the originals by membership overlap (Hungarian assignment), and eigengenes were correlated across retained samples. In **bootstrap** analysis, 100 datasets were drawn with replacement, re-clustered, and compared identically, with 95% confidence intervals from percentiles. Partition-level agreement was summarized by ARI and normalized mutual information (NMI); module-level reproducibility was summarized by the absolute eigengene correlation per module. This distinction — between the stability of exact partition boundaries and the reproducibility of the large eigengene signals — is central to the interpretation and follows established practice in cluster-stability assessment [24].

3.9 Synthesis: the Validate / Replicate-First / Deprioritize framework

All results were integrated into a single, fully quantitative triage applied uniformly to every protein and module (Table 1). A feature earns the highest-priority **Validate** label only if it is directionally consistent across ICM/DCM/HCM against both references, homogeneous ($I^2 < 25\%$ *and* Cochran's Q $p > 0.10$), a member of a stable module (LOHO eigengene $|r| \geq 0.8$), of strong effect (minimum $|\log_2\text{FC}| \geq 0.5$ across all six contrasts), and significant (FDR < 0.05) in *both* main pooled contrasts. **Replicate-First** captures features that are consistent and significant but of moderate heterogeneity ($25\% \leq I^2 < 50\%$), moderate effect ($0.25 \leq \min|\log_2\text{FC}| < 0.5$), or membership in a less-stable module. **Deprioritize** captures the remainder — high heterogeneity ($I^2 \geq 50\%$ or Q $p \leq 0.05$), inconsistent direction, or non-significance in a main contrast.

Table 1: Quantitative decision thresholds for the three-tier triage framework. Protein-level and module-level rules are analogous; modules additionally weight leave-one-heart-out eigengene reproducibility.

Criterion	Validate (highest priority)	Replicate-First / Deprioritize
Directional consistency	Same sign across ICM/DCM/HCM vs both NL and CH	Any sign disagreement → Deprioritize
Heterogeneity	$I^2 < 25\%$ *and* Q $p > 0.10$ (both refs)	$25\% \leq I^2 < 50\%$: Replicate-First; $I^2 \geq 50\%$ or Q $p \leq 0.05$: Deprioritize
Module stability	LOHO eigengene $\|r\| \geq 0.8$ (M1/M2/M3)	M4/M5 (low $\|r\|$) → Replicate-First/Deprioritize
Effect size	$\min\|\log_2\text{FC}| \geq 0.5$ (6 contrasts)	$0.25 \leq \min\|\log_2\text{FC}| < 0.5$: Replicate-First
Significance	FDR < 0.05 in *both* DHF vs NL and DHF vs CH	Not significant in a main contrast → Deprioritize

3.10 Reproducibility and software

The entire pipeline was implemented in Python (3.12) with fixed random seeds. Statistical modeling used ordinary-least-squares fits with a custom limma-faithful empirical-Bayes moderation step; network construction, TOM computation, and clustering used standard scientific-Python libraries. All intermediate matrices, per-feature statistics, stability tables, and figures are retained as analysis artifacts, and the clustering utility was explicitly verified to reproduce the primary module solution (ARI = 1.0) before being reused in the stability analyses.

4 Results

4.1 Cohort composition and quality control

After curation, the analysis cohort comprised 34 LV specimens distributed across the five phenotype groups described above. The filtering cascade reduced the 3,850 MaxQuant protein groups to 2,878 confidently quantified, adequately observed proteins (Table 2), with a post-filter missingness of 10.99% resolved by down-shifted imputation. Per-sample $\log_2$ LFQ intensity distributions were well matched across phenotypes both before and after imputation (Figure 1), confirming that neither systematic sample-loading differences nor the imputation step introduced obvious group-level bias.

Table 2: Reproduced contaminant/decoy and missingness filtering of the processed LFQ matrix.

Filtering step	**Protein groups remaining**
Starting MaxQuant `proteinGroups.txt`	3,850
– Reverse (decoy) hits ($n = 44$)	
– Potential contaminants ($n = 37$)	
– Only-identified-by-site ($n = 67$)	3,713
– Missingness filter ($\geq 70\%$ valid in ≥ 1 group)	**2,878**
Missing values in filtered matrix	10,751 / 97,852 (10.99%)
Imputation (down-shifted normal, $1.8\sigma/0.3\sigma$)	0 missing remain

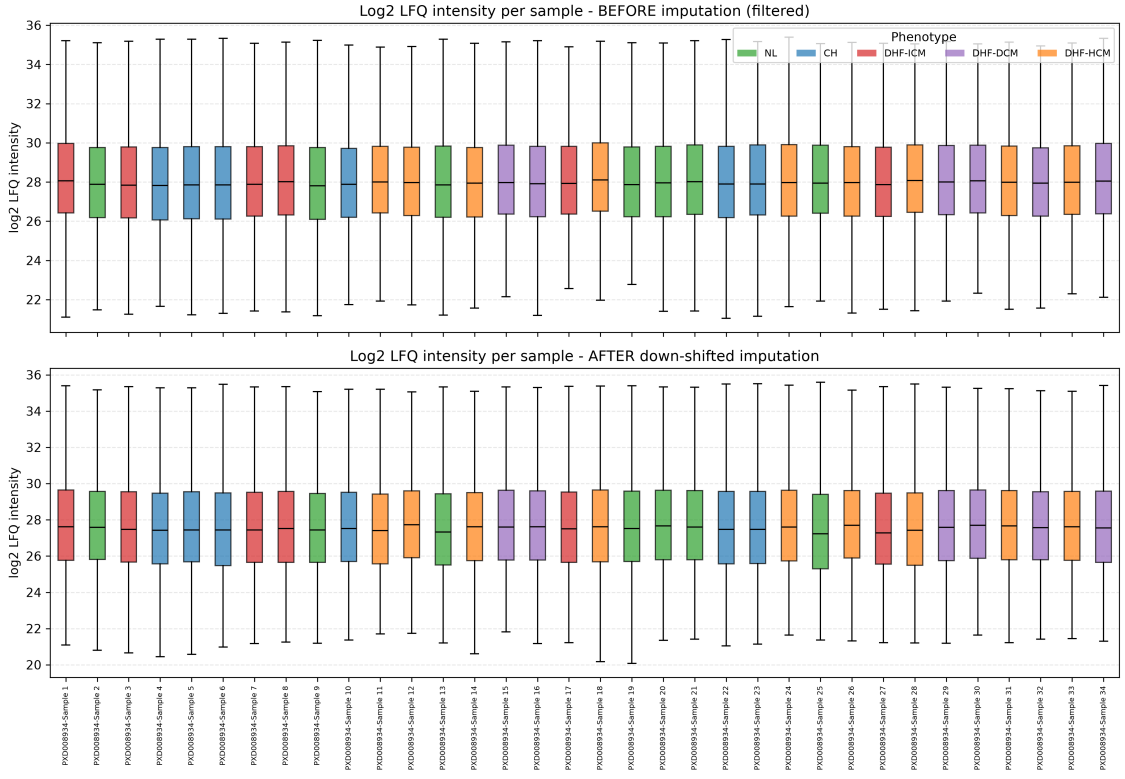

Figure 1: Per-sample $\log_2$ LFQ intensity distributions before (top) and after (bottom) down-shifted imputation, colored by phenotype. Distributions are comparable across the 34 specimens and across phenotype groups, and imputation fills the low-abundance tail without distorting the bulk of each distribution.

4.2 Exploratory structure: non-failing versus decompensated separation

Unsupervised principal-component analysis of the imputed matrix revealed a clear, biologically interpretable gradient (Figure 2). The first principal component (15.7% of variance) separated the non-failing hearts (NL and CH), which cluster toward negative PC1, from the decompensated hearts, which occupy positive PC1 — with the three DHF etiologies interspersed rather than forming three separate islands. This early observation foreshadows the central result: the dominant axis of proteomic variation reflects the failing-versus-non-failing contrast, and it is broadly *shared* across ICM, DCM, and HCM rather than being etiology-specific.

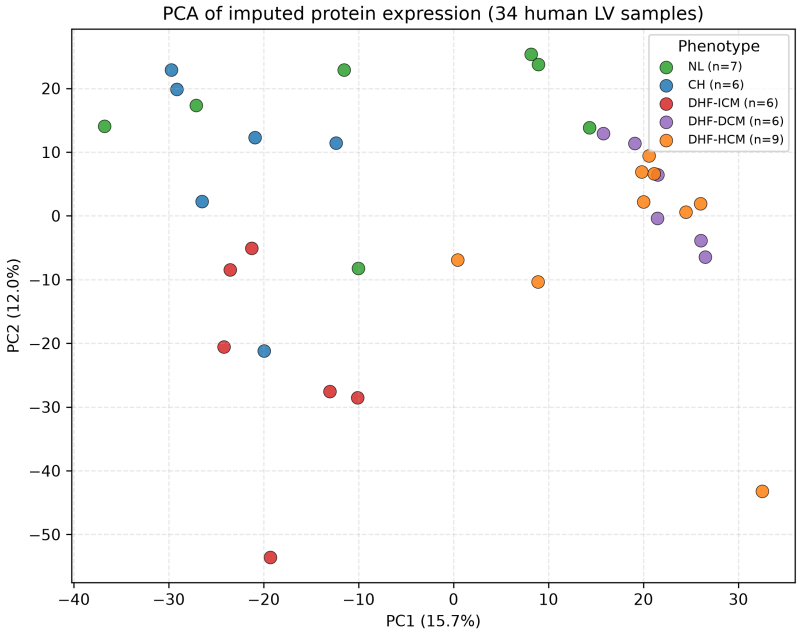

Figure 2: Principal-component analysis of the imputed 34 × 2,878 protein matrix, colored by phenotype. PC1 (15.7%) separates non-failing (NL, CH) from decompensated hearts; the three decompensated etiologies (ICM, DCM, HCM) are interspersed along positive PC1, consistent with a shared decompensation signature.

4.3 Co-abundance modules

Soft-threshold selection identified $\beta = 15$ as the smallest power achieving approximate scale-free topology ($R^2 \geq 0.8$; Figure 3). TOM-based average-linkage clustering resolved five well-separated modules plus a grey unassigned set (Figure 4, Table 3). The two largest modules (M1, 1,139 proteins; M2, 793) capture broad axes of myocardial co-abundance, while the mid-sized M3 (565 proteins) — the focus of this report — and the smaller M4 (92) and M5 (22) capture more specialized programs.

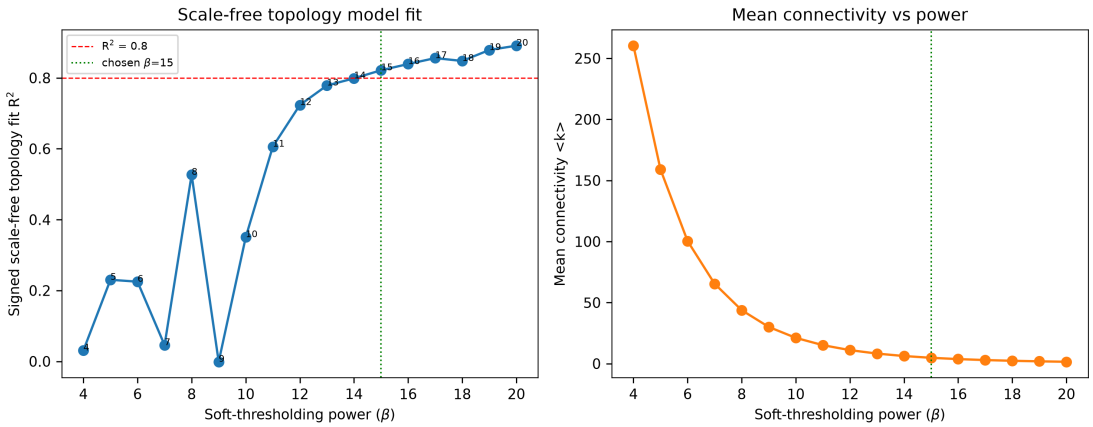

Figure 3: Soft-thresholding power selection. Left: signed scale-free topology model fit R^2 versus power β; the smallest power reaching $R^2 \geq 0.8$ (dashed line) is $\beta = 15$ (dotted line). Right: mean network connectivity $\langle k \rangle$ decreases monotonically with β, reaching $\langle k \rangle = 4.78$ at the chosen power.

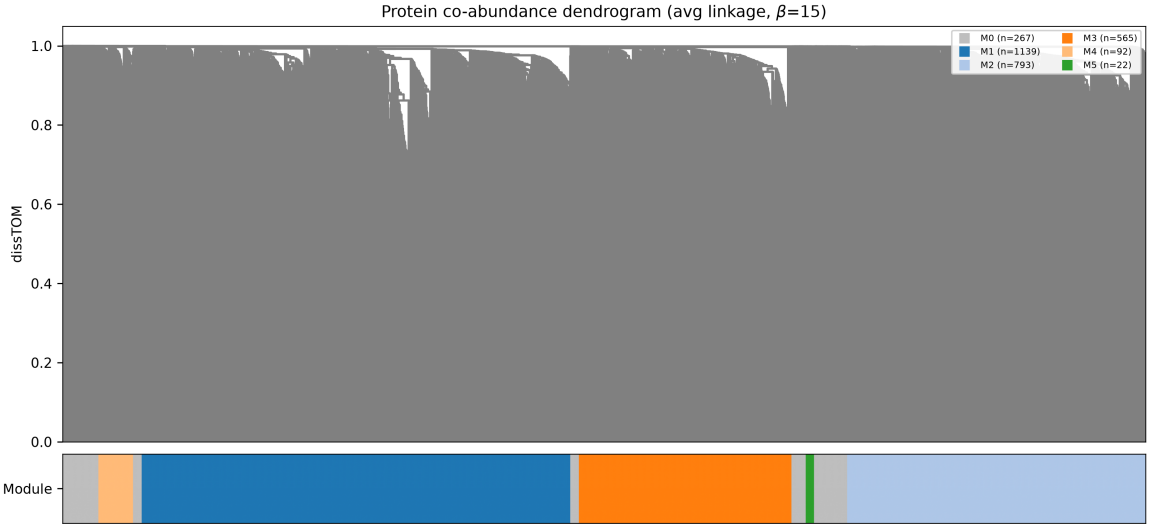

Figure 4: Protein co-abundance dendrogram (average linkage on $1 - \mathrm{TOM}$, $\beta = 15$) with the module color bar beneath. Five modules (M1–M5) plus a grey unassigned set (M0) are resolved.

Table 3: Module sizes and eigengene variance explained. M0 is the grey (unassigned) set.

Module	# proteins	ME var. expl.	Role in this analysis
M1	1,139	0.216	Large; reproducible eigengene but etiology-divergent
M2	793	0.246	Large; reproducible eigengene, down in DHF, heterogeneous
M3	565	0.258	**Up in DHF, pan-etiology homogeneous → Validate**
M4	92	0.274	Consistent but unstable eigengene
M5	22	0.364	Small; unstable and inconsistent
M0	267	—	Grey / unassigned

4.4 Differential abundance: DHF versus non-failing references

Age- and sex-adjusted, EB-moderated contrasts identified a substantial reprogramming of the LV proteome in decompensation (Figure 5). Against NL, 241 proteins reached FDR < 0.05 (158 up, 83 down); against CH, 334 proteins were significant (173 up, 161 down). At the module level, the eigengene of **M3** was significantly up-regulated in *both* contrasts (FDR $= 1.3 \times 10^{-4}$ vs NL; 8.3×10^{-4} vs CH), and **M2** was significantly down-regulated against CH. The most extreme individual proteins are consistent across both references and biologically coherent: the acute-phase proteins *SAA1* and *SAA2* and the inflammatory lectin *LGALS1* are strongly *decreased* in failing tissue, while ECM and plasma-type proteins including *THBS4*, *SERPIND1*, *AHSG*, *CLEC3B*, and *APOA4* are *increased*.

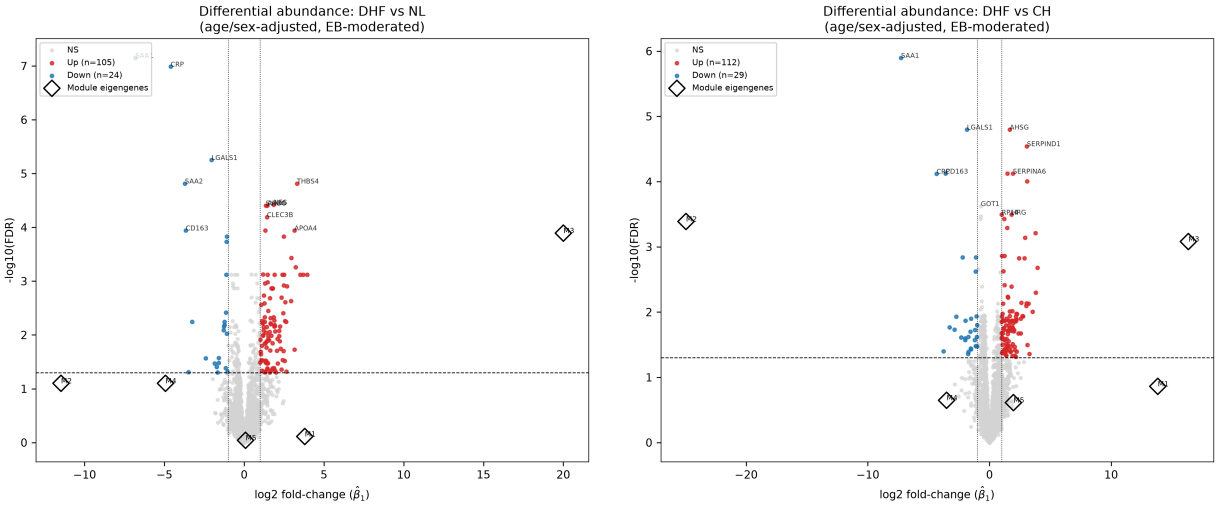

Figure 5: Volcano plots of age/sex-adjusted, EB-moderated differential abundance for DHF vs NL (left) and DHF vs CH (right). Red/blue points are significantly up/down-regulated proteins (FDR < 0.05, $|\log_2 \mathrm{FC}| \geq 1$); the five module eigengenes are overlaid as diamonds. Selected extreme proteins are labeled.

4.5 Cross-etiology consistency and heterogeneity

The defining analysis of this report asks whether module- and protein-level effects hold across all three etiologies. Of the 2,878 proteins, **862 (30%) were directionally consistent** across ICM/DCM/HCM against both references. At the module level, only **M3 and M4** were directionally consistent; critically, **M3 exhibited zero measurable cross-etiology heterogeneity** ($I^2 = 0\%$ for both references; Cochran's Q $p = 0.43$ vs NL, 0.74 vs CH), establishing it as a homogeneous, pan-etiology up-regulation (Figure 6). By contrast, M1 and M2 — despite their large, highly reproducible eigengenes — showed severe heterogeneity ($I^2 = 78$–84%; Q $p < 0.01$), indicating that their eigengene-level behavior *diverges* sharply between etiologies. This is the crucial discriminator: statistical significance and eigengene reproducibility alone do not imply cross-etiology generalizability, and M3 is distinguished precisely by combining all three properties.

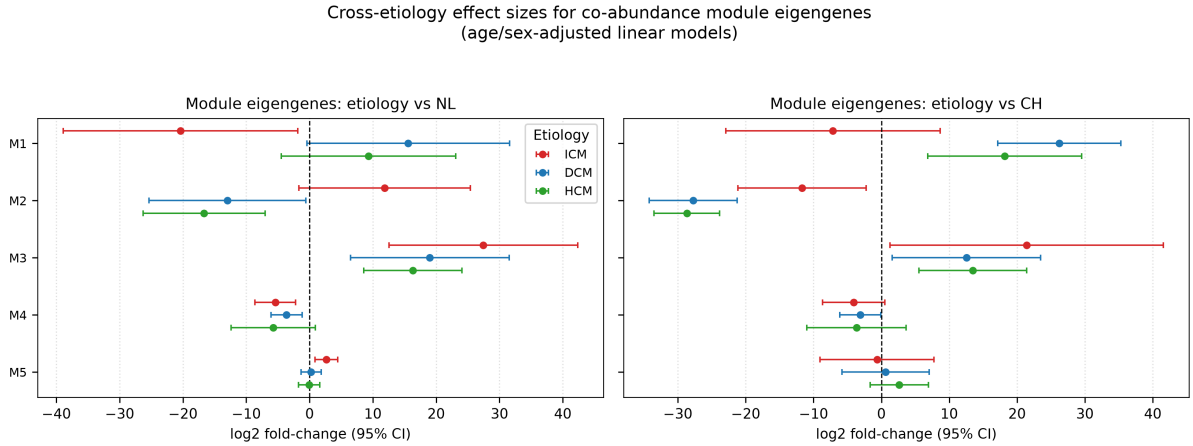

Figure 6: Cross-etiology effect sizes for the five module eigengenes (age/sex-adjusted), against NL (left) and CH (right). Each row shows the per-etiology $\log_2$ fold-change with 95% CI for ICM (red), DCM (blue), and HCM (green). M3's three etiology estimates lie consistently on the same (positive) side with overlapping intervals, whereas M1 and M2 show sign disagreement and wide dispersion across etiologies. Note that eigengene units are on a scaled composite axis and are not directly comparable to single-protein $\log_2$ fold-changes.

At the protein level, the most robustly consistent proteins — ranked by the minimum absolute fold-change across all six contrasts — are dominated by M3 ECM and plasma proteins, led by *SAA1* (M2, down), *CRP* (M2, down), *COL14A1*, *SERPIND1*, *THBS4*, *HBD*, and *SERPINA4* (Figure 7). The forest plots make visually explicit both the strength and the etiologic uniformity of these effects.

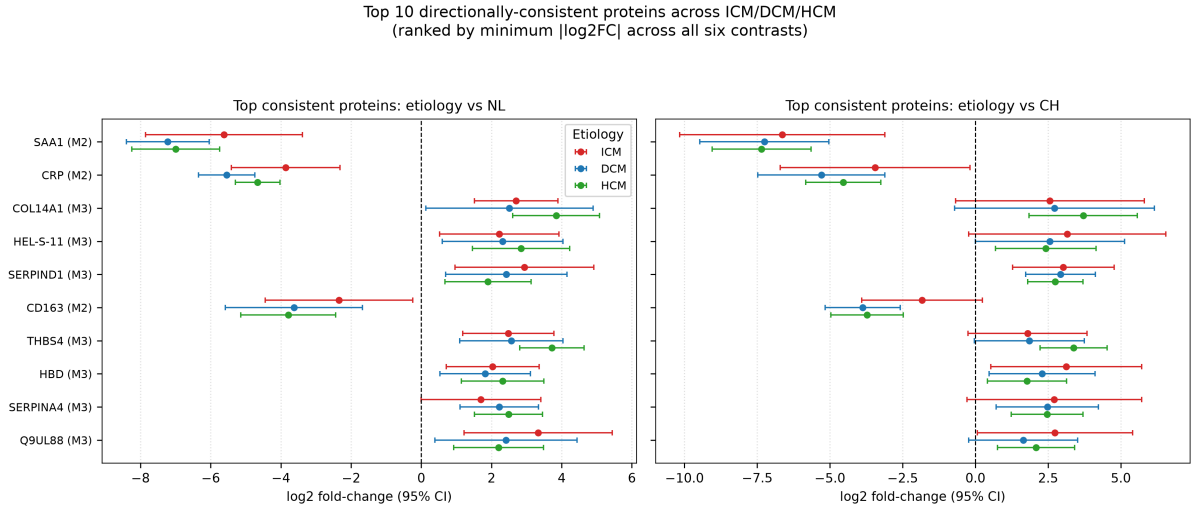

Figure 7: Top-10 directionally-consistent proteins (ranked by minimum $|\log_2 FC|$ across all six contrasts), shown per etiology against NL (left) and CH (right). Point estimates with 95% CIs for ICM (red), DCM (blue), HCM (green). The tight clustering of the three etiology estimates for each protein illustrates the low cross-etiology heterogeneity that underlies Validate status.

4.6 Module stability under resampling

Resampling revealed a clear and interpretable separation between partition-boundary stability and eigengene-signal reproducibility (Table 4). Exact partition agreement was only moderate (LOHO ARI = 0.55; bootstrap ARI = 0.27), as expected for co-abundance networks built from just 34 samples; 31 of 34 LOHO runs nonetheless recovered exactly five modules. However, the *large eigengene signals were highly reproducible*: under LOHO, the M1, M2, and M3 eigengenes recurred

with mean absolute correlations of 0.98, 0.99, and **0.82** respectively, whereas the small M4 and M5 eigengenes were unstable (0.25 and 0.44). The disease-relevant M3 module thus clears the pre-specified stability bar ($|r| \geq 0.8$), while its precise membership boundaries — like those of any module at this sample size — are only moderately determined. The biological conclusion (a reproducible, pan-etiology DHF-up eigengene) is robust even where the fine partition is not.

Table 4: Module partition stability from 34 leave-one-heart-out (LOHO) re-clusterings and 100 bootstrap resamplings. ARI/NMI summarize partition-level agreement; per-module values are mean absolute eigengene correlations.

Metric	LOHO (34 runs)	Bootstrap (100 runs)
Adjusted Rand Index (mean)	0.550 [0.317, 0.688]	0.268 [0.124, 0.435]
Normalized mutual information	0.467	0.222
Runs recovering 5 modules	31 / 34	61 / 100
M1 eigengene $\|r\|$	0.98	0.88
M2 eigengene $\|r\|$	0.99	0.91
M3 eigengene $\|r\|$	**0.82**	**0.56**
M4 eigengene $\|r\|$	0.25	0.36
M5 eigengene $\|r\|$	0.44	0.16

4.7 Integrated classification: modules and proteins

Applying the triage framework uniformly (Table 5) yields a single Validate module, **M3**, which satisfies every criterion: stable eigengene (LOHO $r = 0.82$), directional consistency, homogeneity ($I^2 = 0\%$), and significance in both main contrasts. **M2** is graded *Replicate-First*: its eigengene is the most reproducible of all (LOHO $r = 0.99$) and it is significant against CH, but its cross-etiology heterogeneity ($I^2 \approx 82\%$) precludes Validate status. Modules **M1**, **M4**, and **M5** are *Deprioritized* for heterogeneity (M1), eigengene instability (M4, M5), or non-significance.

Table 5: Module-level classification. FDR values are for the module eigengene in the pooled DHF contrasts. "LOHO r" is the mean absolute leave-one-heart-out eigengene correlation.

Module	n	Class	LOHO r	Consistent?	I^2 (NL/CH)	Dir.	Basis
M3	565	**Validate**	0.82	Yes	0%/0%	up	Stable, homogeneous, sig. both
M2	793	**Replicate-First**	0.99	No	83%/81%	down	Reproducible but heterogeneous
M1	1,139	Deprioritize	0.98	No	78%/84%	up	Etiology-divergent
M4	92	Deprioritize	0.25	Yes	0%/0%	down	Unstable eigengene; NS
M5	22	Deprioritize	0.44	No	64%/0%	up	Unstable; inconsistent; NS

At the protein level, the framework labels **31 proteins Validate, 44 Replicate-First, and 2,803 Deprioritize**. The Validate set is overwhelmingly an M3 phenomenon: 27 of the 31 Validate proteins reside in M3, with 3 in M2 and 1 in M1. The top-20 Validate candidates, ranked by their minimum guaranteed effect across all six contrasts, are listed in Table 6 and displayed as a cross-etiology effect heatmap in Figure 8. The heatmap makes the core result immediately legible: *SAA1* is uniformly, strongly negative across all six contrasts (deep blue), while the M3 candidates form a coherent block of positive fold-changes (red) that is stable in sign and comparable in magnitude across ICM, DCM, and HCM and against both references.

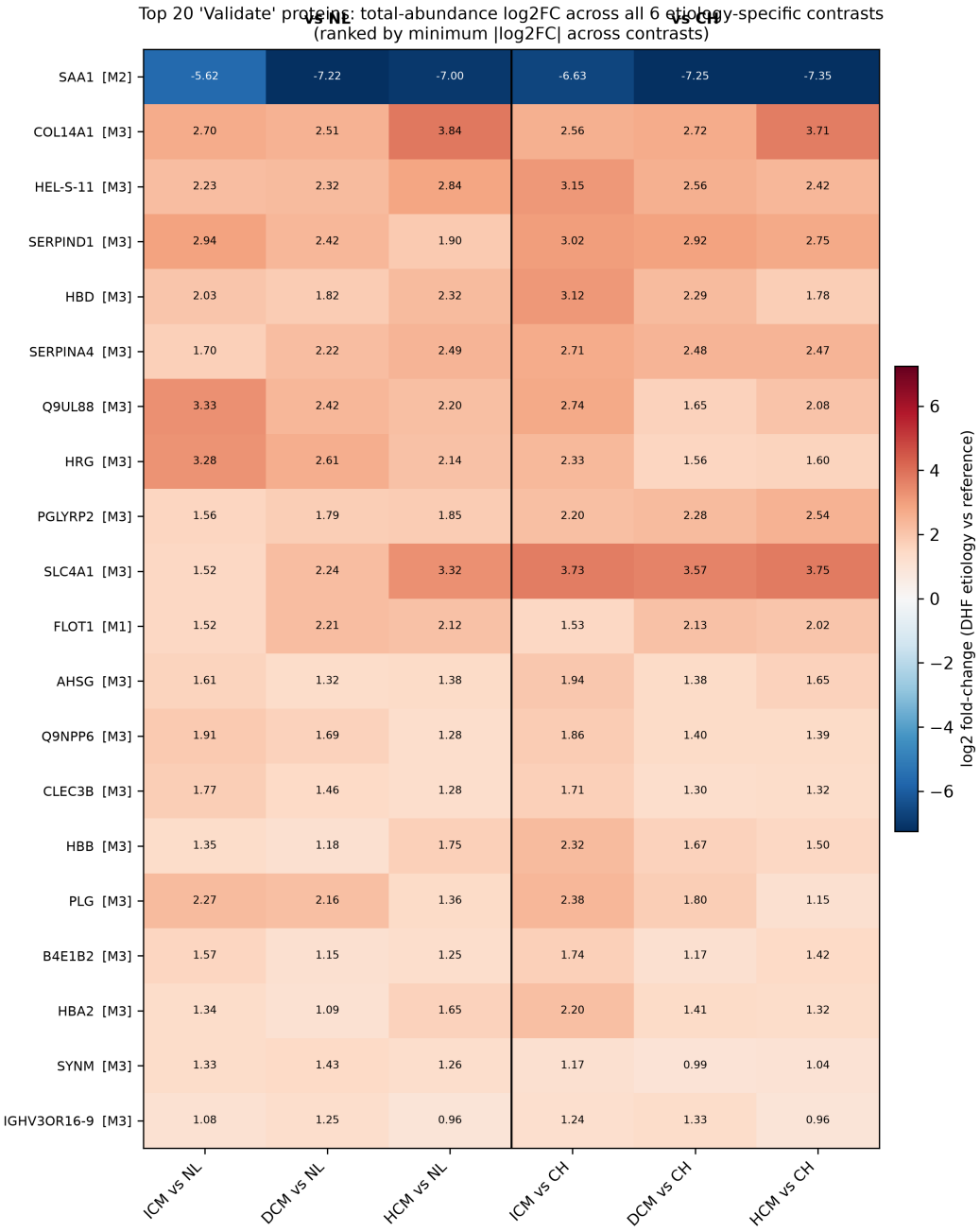

Figure 8: Cross-etiology effect heatmap for the top-20 Validate candidates. Columns are the six etiology-specific contrasts (ICM/DCM/HCM vs NL, then vs CH; vertical separator); rows are proteins annotated by module. Cell color encodes the total-abundance $\log_2$ fold-change (red up, blue down). *SAA1* (M2) is consistently down; the M3-dominated remainder is consistently up, with directionally uniform effects across all etiologies and both references.

Table 6: Top-20 Validate candidate proteins, ranked by the minimum absolute $\log_2$ fold-change across all six etiology-specific contrasts (i.e., the weakest guaranteed effect). "Dir." is the consistent direction; FDR values are for the two pooled DHF contrasts. All values are total protein abundance; no PTM is inferred.

#	Gene	Module	Dir.	min |lfc|	mean |lfc|	FDR vs NL	FDR vs CH
1	*SAA1*	M2	down	5.62	6.85	7.1×10^{-8}	1.3×10^{-6}
2	*COL14A1*	M3	up	2.51	3.01	7.6×10^{-4}	9.8×10^{-3}
3	*HEL-S-11/CA1*	M3	up	2.23	2.59	3.7×10^{-4}	1.3×10^{-2}
4	*SERPIND1*	M3	up	1.90	2.66	2.0×10^{-3}	2.9×10^{-5}
5	*HBD*	M3	up	1.78	2.23	7.6×10^{-4}	1.4×10^{-2}
6	*SERPINA4*	M3	up	1.70	2.34	1.2×10^{-3}	7.2×10^{-3}
7	*Q9UL88* (ADAR-assoc.)	M3	up	1.65	2.40	2.5×10^{-3}	1.1×10^{-2}
8	*HRG*	M3	up	1.56	2.25	7.6×10^{-4}	3.2×10^{-4}
9	*PGLYRP2*	M3	up	1.56	2.04	1.4×10^{-2}	1.5×10^{-3}
10	*SLC4A1*	M3	up	1.52	3.02	5.5×10^{-4}	6.2×10^{-4}
11	*FLOT1*	M1	up	1.52	1.92	2.0×10^{-2}	3.4×10^{-2}
12	*AHSG*	M3	up	1.32	1.55	3.9×10^{-5}	1.6×10^{-5}
13	*Q9NPP6*	M3	up	1.28	1.59	1.0×10^{-2}	5.8×10^{-3}
14	*CLEC3B*	M3	up	1.28	1.47	6.4×10^{-5}	5.1×10^{-4}
15	*HBB*	M3	up	1.18	1.63	1.4×10^{-3}	1.4×10^{-2}
16	*PLG*	M3	up	1.15	1.85	4.8×10^{-3}	1.9×10^{-2}
17	*B4E1B2*	M3	up	1.15	1.38	1.1×10^{-4}	7.6×10^{-5}
18	*HBA2/HBA1*	M3	up	1.09	1.50	1.4×10^{-3}	1.9×10^{-2}
19	*SYNM*	M3	up	0.99	1.20	3.9×10^{-5}	7.4×10^{-3}
20	*IGHV3OR16-9*	M3	up	0.96	1.14	1.0×10^{-2}	2.4×10^{-3}

5 Discussion and Synthesis

5.1 Module M3 as a coherent, pan-etiology decompensation signature

The central result of this re-analysis is that a single co-abundance module, M3, satisfies every quantitative criterion for prioritized experimental follow-up: it is coordinately up-regulated in decompensated myocardium relative to both non-failing references, it is directionally uniform across three mechanistically distinct etiologies with statistically undetectable heterogeneity, and its eigengene is reproducible under leave-one-heart-out resampling. The biological character of M3 is that of a matrix-remodeling and plasma/acute-phase program. Its highest-ranked, most robustly consistent resident-tissue member is *COL14A1*, a fibril-associated collagen (FACIT family) that regulates collagen fibrillogenesis and is required for the structural integrity of the myocardium; loss of collagen XIV in murine models produces disorganized ECM and heightened susceptibility to adverse remodeling under hemodynamic stress [25]. Human transcriptomic and proteomic surveys have independently identified *COL14A1* among the collagen genes induced during cardiac remodeling and fibrosis [26, 27]. Its coordinated rise here, together with the matricellular protein *THBS4* — itself a well-established regulator of pressure-overload fibrosis and remodeling [28, 29] — positions M3 as a proteomic correlate of the fibrotic, matrix-stiffening axis that is a shared endpoint of ICM, DCM, and HCM decompensation [7].

5.2 The congestion and blood-retention caveat

A sober interpretation of M3 must confront the composition of its top candidates. Beyond *COL14A1* and *SYNM*, the leading Validate proteins are overwhelmingly abundant plasma, coagulation, and erythrocyte proteins: *SERPIND1* (heparin cofactor II), *SERPINA4* (kallistatin), *HRG*, *AHSG* (fetuin-A), *PLG* (plasminogen), *CLEC3B* (tetranectin), and the hemoglobins *HBB*, *HBA2*, and *HBD*, alongside the erythrocyte anion transporter *SLC4A1* (band 3) and carbonic anhydrase *CA1*. The coordinated elevation of this ensemble in decompensated hearts is biologically expected but mechanistically ambiguous: decompensation is defined in part by systemic and intramyocardial *congestion*, venous pressure elevation, and edema [30], and a myocardial biopsy from a congested,

blood-laden failing heart will contain more trapped plasma and erythrocyte content than a well-perfused donor heart. A meaningful portion of the M3 "signal" may therefore report the *physiological state of congestion* rather than a change in cardiomyocyte- or fibroblast-intrinsic protein expression. This does not diminish M3's value as a robust, pan-etiology *severity signature*; it does, however, mandate that mechanistic claims be reserved for candidates with plausible resident-cell biology — principally *COL14A1* (fibroblast/ECM), *SYNM* (a cardiomyocyte intermediate-filament protein that co-assembles with desmin) [31], and *FLOT1* (a membrane-microdomain scaffold) — and that all validation be accompanied by explicit hemoglobin/blood-content covariates to separate resident expression from congestion.

5.3 The acute-phase axis and the deprioritization of CRP

The most extreme single protein in the entire analysis is *SAA1* (serum amyloid A), which is strongly and uniformly *decreased* in failing myocardium across all six contrasts. Serum amyloid A is a classical hepatically-derived acute-phase apolipoprotein with well-documented associations to cardiovascular risk [32]; its consistent tissue-level reduction here, mirrored by *CRP*, is intriguing and reproducible, and *SAA1* attains protein-level Validate status through the high eigengene reproducibility of its host module M2. Yet the fate of *CRP* in our framework is instructive. Despite being highly significant and directionally consistent — and despite the strong prior literature linking C-reactive protein to heart-failure risk and outcomes [33] — *CRP* is **quantitatively deprioritized** because its magnitude is heterogeneous across etiologies ($I^2 \approx 58\%$). This is exactly the discipline the framework is designed to enforce: biological plausibility and nominal significance are not sufficient; a top candidate must also generalize in *magnitude*, not merely in sign, across the disease spectrum. *CRP* is accordingly retained as an inflammatory reference marker rather than a lead target.

5.4 Why reproducible, significant modules can still fail the test

Modules M1 and M2 provide the analysis's most important methodological lesson. Both possess extremely reproducible eigengenes (LOHO $|r| = 0.98$ and 0.99) and M2 is significantly altered against CH — properties that, in a conventional single-cohort analysis, might elevate them to top candidacy. However, both are severely *etiology-divergent* ($I^2 \approx 78$–84%; Cochran's Q $p < 0.01$), meaning their eigengene moves in different directions or magnitudes depending on whether the failing heart is ischemic, dilated, or hypertrophic. Fetuin-A biology offers a concrete illustration of why such divergence matters: *AHSG* exerts context-dependent, tissue-specific effects on calcification and remodeling [34], and a protein embedded in an etiology-divergent module cannot be assumed to behave uniformly across diseases. The framework therefore correctly routes M2 to Replicate-First and M1 to Deprioritize, reserving Validate for the one module — M3 — that combines reproducibility, significance, *and* cross-etiology homogeneity. This tripartite requirement is the analytical core of the report and the reason its recommendation is defensible.

5.5 Relationship to the original study and limitations

Because `PXD008934` was generated to study detyrosinated-microtubule mechanics [1], our network-level, cross-etiology triage is genuinely orthogonal to the source publication and does not attempt to reproduce or contest its cytoskeletal conclusions. Several limitations bound our own claims. The cohort is small ($n = 34$), which limits the stability of exact module boundaries (reflected in the moderate ARI values) and the precision of per-etiology estimates, particularly for the composite HCM group. Down-shifted imputation, although standard, can influence low-abundance inferences [19]. Module eigengene fold-changes are expressed on a scaled composite axis and are not directly comparable to single-protein $\log_2$ fold-changes, so we base magnitude claims on protein-level effects. Most fundamentally, the data are protein-group-level LFQ intensities: they report *total abundance* and nothing about phosphorylation, glycosylation, proteolytic processing,

or any other modification. No PTM inference is made anywhere in this work, and the validation plan below is engineered to preserve that boundary.

6 Orthogonal Experimental Validation Plan

The discovery analysis nominates module M3 and a compact list of proteins for confirmation. Because the discovery data are LFQ intensities, the validation program is designed around three principles: orthogonality of measurement platform, biological replication in independent human tissue, and strict confinement to total protein abundance. The plan is tiered (Table 7) and its success criteria are pre-registered.

Non-negotiable design constraint: total abundance only, no PTM inference

Every assay below quantifies **total protein abundance**. Targeted-MS peptides are selected to be proteotypic, fully tryptic, and *modification-independent*, explicitly excluding sequences overlapping annotated modification sites; antibody assays use validated pan (modification-independent) reagents. Any discrepancy between platforms is **not** to be attributed to a PTM without a separate, PTM-specific experiment that lies outside the scope of this abundance-validation plan.

6.1 Tier 1 — Targeted mass spectrometry (orthogonal absolute quantification)

The primary confirmatory platform is **parallel reaction monitoring (PRM)** on a high-resolution Q-Orbitrap for the full Validate + Replicate-First panel, with a focused subset cross-validated by **selected reaction monitoring (SRM/MRM)** on a triple quadrupole to demonstrate platform independence [35–37]. Quantification is made absolute using stable-isotope-labeled (SIL/AQUA) internal-standard peptides spiked at known concentrations. For each target, at least two to three proteotypic, modification-independent tryptic peptides are selected and verified for uniqueness against the human proteome. Measurements are taken in human LV free-wall myocardium (the same anatomical region as discovery), and results are reported both as SIL-based absolute concentrations and as ratios normalized to invariant myocardial reference proteins. Critically, a **hemoglobin/blood-content covariate** (PRM signal for *HBB*/*HBA2*) is measured for every specimen and included in the statistical model, so that resident-expression effects can be distinguished from congestion. Two cohorts are used: where residual material exists, the original `PXD008934` specimens (technical LFQ-vs-PRM concordance), and, as the definitive test, an *independent* set of NL/CH/ICM/DCM/HCM LV specimens (biological replication). The six etiology-specific contrasts and the two pooled contrasts are re-computed, and cross-etiology I^2/Cochran's Q are re-estimated to confirm the low-heterogeneity property that defines the Validate set.

6.2 Tier 2 — Antibody-based, MS-independent confirmation

The highest-confidence subset (*COL14A1*, *SERPIND1*, *SERPINA4*, *HRG*, *AHSG*, *CLEC3B*, *SYNM*, *FLOT1*, *SAA1*, and *CRP* as an inflammatory reference) is confirmed by assays that share none of the biases of mass spectrometry. Semi-quantitative **Western blotting** of LV lysates uses total-protein normalization (stain-free/REVERT rather than a single housekeeping band, to avoid heart-failure-associated housekeeping drift) and validated pan antibodies, with recombinant-protein and knockdown/knockout specificity controls. Quantitative **ELISA** (or automated capillary immunoassay) is applied to the secreted/plasma-type candidates on tissue homogenate and, where available, matched plasma, to test biomarker potential and disentangle circulating from tissue-resident contributions. Finally, **immunohistochemistry/immunofluorescence** on LV sections establishes cell-type localization — co-staining *COL14A1* with fibroblast/collagen markers, *SYNM* with cardiomyocyte markers, and the plasma-type candidates with erythrocyte/vascular markers — providing a direct, spatial test of the congestion-versus-resident-expression hypothesis.

6.3 Tier 3 — Functional interrogation

Functional follow-up is reserved for candidates with plausible resident-cell mechanisms, while plasma-derived candidates are treated as severity biomarkers. In human induced-pluripotent-stem-cell-derived cardiomyocytes (iPSC-CMs) and cardiac fibroblasts [38, 39], neurohormonal and mechanical stressors (endothelin-1, phenylephrine, angiotensin II, isoproterenol; stretch; hypoxia) model decompensation, and loss- and gain-of-function (CRISPRi/knockout and overexpression) of *COL14A1*, *SYNM*, and *FLOT1* are read out for fibrosis/ECM programs, hypertrophy and contractility, and inflammatory signaling; three-dimensional engineered heart tissue confirms mechanical consequences. In vivo, etiology-diverse models — transverse aortic constriction (pressure overload) [40], coronary ligation (ischemic failure), and a genetic HCM model — with cardiomyocyte- or fibroblast-specific conditional manipulation test whether modulating a top candidate alters function, fibrosis, and remodeling, with target engagement confirmed by PRM (again, total abundance only). Optional human-genetic triangulation (cardiac cis-pQTL/eQTL, Mendelian randomization) can seek orthogonal evidence for causality versus reactivity. In parallel, the Validate candidate set is interrogated for pathway and biological-process over-representation using curated proteomics enrichment resources [41] to prioritise mechanistically coherent subsets for the wet-lab experiments above.

Table 7: Tiered validation plan with pre-registered success criteria. All measurements quantify total protein abundance.

Tier	Approach	Pre-registered success criterion
Tier 1: Targeted MS	PRM (+ SRM cross-check), SIL absolute quant, independent LV cohort, hemoglobin covariate	Same sign & FDR < 0.05 in pooled DHF for $\geq 80\%$ of Validate candidates; M3 candidates concordant across ICM/DCM/HCM; replication $I^2 < 25\%$; effect survives blood-content adjustment for resident-claimed candidates
Tier 2: Antibody assays	Western (total-protein normalized), ELISA (tissue + plasma), IHC/IF localization	Concordant direction for the high-confidence subset; cell-type localization consistent with proposed biology
Tier 3: Functional	iPSC-CM/fibroblast ± EHT; TAC / MI / HCM in vivo; genetic triangulation	Perturbation of ≥ 1 resident candidate (*COL14A1*/*SYNM*/*FLOT1*) yields a direction-consistent remodeling/fibrosis phenotype in vitro and in ≥ 1 in vivo model

7 Conclusion

A reproducible, network-level re-analysis of the human LV proteome in `PXD008934` identifies module **M3** — an ECM/plasma acute-phase program up-regulated in decompensation — as the single co-abundance module that is simultaneously reproducible, significant against both non-failing references, and directionally homogeneous across ischemic, dilated, and hypertrophic etiologies. Of 2,878 quantified proteins, 31 meet the highest-priority Validate criteria (27 in M3), led by *COL14A1*, *SERPIND1*, *SERPINA4*, *HRG*, *AHSG*, *CLEC3B*, *PLG*, and *SYNM*, with *SAA1* (uniformly down) and *FLOT1* qualifying through their modules' reproducibility. The recommendation is deliberately disciplined: reproducibility and significance are necessary but not sufficient, and candidates such as *CRP* and the entirety of module M2 are down-graded precisely because their effects do not generalize in magnitude across etiologies. Two caveats — the congestion/blood-retention origin

of many plasma-type candidates and the abundance-only nature of the data — are built directly into the tiered validation plan, which prioritizes resident-cell candidates, embeds hemoglobin covariates, and rigorously excludes any inference of post-translational modification. M3 and its leading proteins constitute a compact, testable, pan-etiology hypothesis for the molecular signature of cardiac decompensation.

Data and Code Availability

The primary data are publicly available from the EBI PRIDE Archive under accession PXD008934 (revision 3). All derived matrices (filtered and imputed expression, module assignments, eigengenes), per-feature statistics (differential abundance, cross-etiology heterogeneity, stability), the full candidate classification table, and all figures are retained as analysis artifacts accompanying this report. Effect sizes throughout are total protein-abundance $\log_2$ fold-changes; no post-translational modification is measured or inferred.

References

[1] Christina Yingxian Chen, Matthew A. Caporizzo, Kenneth Bedi, Alexia Vite, Alexey I. Bogush, Patrick Robison, Julie G. Heffler, Alex K. Salomon, Neil A. Kelly, Apoorva Babu, Michael P. Morley, Kenneth B. Margulies, and Benjamin L. Prosser. Suppression of detyrosinated microtubules improves cardiomyocyte function in human heart failure. *Nature Medicine*, 24(8):1225–1233, June 2018. ISSN 1546-170X. doi: 10.1038/s41591-018-0046-2. URL http://dx.doi.org/10.1038/s41591-018-0046-2.

[2] Gianluigi Savarese, Peter Moritz Becher, Lars H Lund, Petar Seferovic, Giuseppe M C Rosano, and Andrew J S Coats. Global burden of heart failure: a comprehensive and updated review of epidemiology. *Cardiovascular Research*, 118(17):3272–3287, February 2022. ISSN 1755-3245. doi: 10.1093/cvr/cvac013. URL http://dx.doi.org/10.1093/cvr/cvac013.

[3] Theresa A McDonagh, Marco Metra, Marianna Adamo, Roy S Gardner, Andreas Baumbach, Michael Böhm, Haran Burri, Javed Butler, Jelena Čelutkienė, Ovidiu Chioncel, John G F Cleland, Andrew J S Coats, Maria G Crespo-Leiro, Dimitrios Farmakis, Martine Gilard, Stephane Heymans, Arno W Hoes, Tiny Jaarsma, Ewa A Jankowska, Mitja Lainscak, Carolyn S P Lam, Alexander R Lyon, John J V McMurray, Alexandre Mebazaa, Richard Mindham, Claudio Muneretto, Massimo Francesco Piepoli, Susanna Price, Giuseppe M C Rosano, Frank Ruschitzka, Anne Kathrine Skibelund, Rudolf A de Boer, P Christian Schulze, Magdy Abdelhamid, Victor Aboyans, Stamatis Adamopoulos, Stefan D Anker, Elena Arbelo, Riccardo Asteggiano, Johann Bauersachs, Antoni Bayes-Genis, Michael A Borger, Werner Budts, Maja Cikes, Kevin Damman, Victoria Delgado, Paul Dendale, Polychronis Dilaveris, Heinz Drexel, Justin Ezekowitz, Volkmar Falk, Laurent Fauchier, Gerasimos Filippatos, Alan Fraser, Norbert Frey, Chris P Gale, Finn Gustafsson, Julie Harris, Bernard Iung, Stefan Janssens, Mariell Jessup, Aleksandra Konradi, Dipak Kotecha, Ekaterini Lambrinou, Patrizio Lancellotti, Ulf Landmesser, Christophe Leclercq, Basil S Lewis, Francisco Leyva, Aleš Linhart, Maja-Lisa Løchen, Lars H Lund, Donna Mancini, Josep Masip, Davor Milicic, Christian Mueller, Holger Nef, Jens-Cosedis Nielsen, Lis Neubeck, Michel Noutsias, Steffen E Petersen, Anna Sonia Petronio, Piotr Ponikowski, Eva Prescott, Amina Rakisheva, Dimitrios J Richter, Evgeny Schlyakhto, Petar Seferovic, Michele Senni, Marta Sitges, Miguel Sousa-Uva, Carlo G Tocchetti, Rhian M Touyz, Carsten Tschoepe, Johannes Waltenberger, Marianna Adamo, Andreas Baumbach, Michael Böhm, Haran Burri, Jelena Čelutkienė, Ovidiu Chioncel, John G F Cleland, Andrew J S Coats, Maria G Crespo-Leiro, Dimitrios Farmakis, Roy S Gardner, Martine Gilard, Stephane Heymans, Arno W Hoes, Tiny Jaarsma, Ewa A Jankowska, Mitja Lainscak, Carolyn S P Lam, Alexander R Lyon, John J V McMurray, Alexandre Mebazaa, Richard Mindham, Claudio Muneretto, Massimo Francesco Piepoli, Susanna Price, Giuseppe M C Rosano, Frank Ruschitzka, and Anne Kathrine Skibelund. 2021 esc guidelines for the diagnosis and treatment of acute and chronic heart failure. *European Heart Journal*, 42(36):3599–3726, August 2021. ISSN 1522-9645. doi: 10.1093/eurheartj/ehab368. URL http://dx.doi.org/10.1093/eurheartj/ehab368.

[4] Michinari Nakamura and Junichi Sadoshima. Mechanisms of physiological and pathological cardiac hypertrophy. *Nature Reviews Cardiology*, 15(7):387–407, April 2018. ISSN 1759-5010. doi: 10.1038/s41569-018-0007-y. URL http://dx.doi.org/10.1038/s41569-018-0007-y.

[5] Gabriele G. Schiattarella and Joseph A. Hill. Inhibition of hypertrophy is a good therapeutic strategy in ventricular pressure overload. *Circulation*, 131(16):1435–1447, April 2015. ISSN 1524-4539. doi: 10.1161/circulationaha.115.013894. URL http://dx.doi.org/10.1161/CIRCULATIONAHA.115.013894.

[6] Liyan Zhang, Jagdip S. Jaswal, John R. Ussher, Sowndramalingam Sankaralingam, Cory Wagg, Michael Zaugg, and Gary D. Lopaschuk. Cardiac insulin-resistance and decreased mitochondrial energy production precede the development of systolic heart failure after pressure-overload hypertrophy. *Circulation: Heart Failure*, 6(5):1039–1048, September 2013. ISSN 1941-3297. doi: 10.1161/circheartfailure.112.000228. URL http://dx.doi.org/10.1161/CIRCHEARTFAILURE.112.000228.

[7] Nikolaos G. Frangogiannis. The inflammatory response in myocardial injury, repair, and remodelling. *Nature Reviews Cardiology*, 11(5):255–265, March 2014. ISSN 1759-5010. doi: 10.1038/nrcardio.2014.28. URL http://dx.doi.org/10.1038/nrcardio.2014.28.

[8] Paola Pastena, Jesse T. Frye, Carson Ho, Marc E. Goldschmidt, and Andreas P. Kalogeropoulos. Ischemic cardiomyopathy: epidemiology, pathophysiology, outcomes, and therapeutic options. *Heart Failure Reviews*, 29(1):287–299, December 2023. ISSN 1573-7322. doi: 10.1007/s10741-023-10377-4. URL http://dx.doi.org/10.1007/s10741-023-10377-4.

[9] Steve R. Ommen, Carolyn Y. Ho, Irfan M. Asif, Seshadri Balaji, Michael A. Burke, Sharlene M. Day, Joseph A. Dearani, Kelly C. Epps, Lauren Evanovich, Victor A. Ferrari, José A. Joglar, Sadiya S. Khan, Jeffrey J. Kim, Michelle M. Kittleson, Chayakrit Krittanawong, Matthew W. Martinez, Seema Mital, Srihari S. Naidu, Sara Saberi, Christopher Semsarian, Sabrina Times, and Cynthia Burstein Waldman. 2024 aha/acc/amssm/hrs/paces/scmr guideline for the management of hypertrophic cardiomyopathy: A report of the american heart association/american college of cardiology joint committee on clinical practice guidelines. *Circulation*, 149(23), June 2024. ISSN 1524-4539. doi: 10.1161/cir.0000000000001250. URL http://dx.doi.org/10.1161/CIR.0000000000001250.

[10] Sophia Doll, Martina Dreßen, Philipp E. Geyer, Daniel N. Itzhak, Christian Braun, Stefanie A. Doppler, Florian Meier, Marcus-Andre Deutsch, Harald Lahm, Rüdiger Lange, Markus Krane, and Matthias Mann. Region and cell-type resolved quantitative proteomic map of the human heart. *Nature Communications*, 8(1), November 2017. ISSN 2041-1723. doi: 10.1038/s41467-017-01747-2. URL http://dx.doi.org/10.1038/s41467-017-01747-2.

[11] Bin Zhang and Steve Horvath. A general framework for weighted gene co-expression network analysis. *Statistical Applications in Genetics and Molecular Biology*, 4(1), January 2005. ISSN 2194-6302. doi: 10.2202/1544-6115.1128. URL http://dx.doi.org/10.2202/1544-6115.1128.

[12] Peter Langfelder and Steve Horvath. Wgcna: an r package for weighted correlation network analysis. *BMC Bioinformatics*, 9(1), December 2008. ISSN 1471-2105. doi: 10.1186/1471-2105-9-559. URL http://dx.doi.org/10.1186/1471-2105-9-559.

[13] Gordon K Smyth. Linear models and empirical bayes methods for assessing differential expression in microarray experiments. *Statistical Applications in Genetics and Molecular Biology*, 3(1):1–25, January 2004. ISSN 1544-6115. doi: 10.2202/1544-6115.1027. URL http://dx.doi.org/10.2202/1544-6115.1027.

[14] Matthew E. Ritchie, Belinda Phipson, Di Wu, Yifang Hu, Charity W. Law, Wei Shi, and Gordon K. Smyth. limma powers differential expression analyses for rna-sequencing and microarray studies. *Nucleic Acids Research*, 43(7):e47–e47, January 2015. ISSN 0305-1048. doi: 10.1093/nar/gkv007. URL http://dx.doi.org/10.1093/nar/gkv007.

[15] Yasset Perez-Riverol, Jingwen Bai, Chakradhar Bandla, David García-Seisdedos, Suresh Hewapathirana, Selvakumar Kamatchinathan, Deepti J Kundu, Ananth Prakash, Anika Frericks-Zipper, Martin Eisenacher, Mathias Walzer, Shengbo Wang, Alvis Brazma, and Juan Antonio Vizcaíno. The pride database resources in 2022: a hub for mass spectrometry-based proteomics evidences. *Nucleic Acids Research*, 50(D1):D543–D552, November 2021. ISSN 1362-4962. doi: 10.1093/nar/gkab1038. URL http://dx.doi.org/10.1093/nar/gkab1038.

[16] Juan A Vizcaíno, Eric W Deutsch, Rui Wang, Attila Csordas, Florian Reisinger, Daniel Ríos, José A Dianes, Zhi Sun, Terry Farrah, Nuno Bandeira, Pierre-Alain Binz, Ioannis Xenarios, Martin Eisenacher, Gerhard Mayer, Laurent Gatto, Alex Campos, Robert J Chalkley, Hans-Joachim Kraus, Juan Pablo Albar, Salvador Martinez-Bartolomé, Rolf Apweiler, Gilbert S Omenn, Lennart Martens, Andrew R Jones, and Henning Hermjakob. Proteomexchange provides globally coordinated proteomics data submission and dissemination. *Nature Biotechnology*, 32(3):223–226, March 2014. ISSN 1546-1696. doi: 10.1038/nbt.2839. URL http://dx.doi.org/10.1038/nbt.2839.

[17] Jürgen Cox and Matthias Mann. Maxquant enables high peptide identification rates, individualized p.p.b.-range mass accuracies and proteome-wide protein quantification. *Nature Biotechnology*, 26(12): 1367–1372, November 2008. ISSN 1546-1696. doi: 10.1038/nbt.1511. URL http://dx.doi.org/10.1038/nbt.1511.

[18] Stefka Tyanova, Tikira Temu, Pavel Sinitcyn, Arthur Carlson, Marco Y Hein, Tamar Geiger, Matthias Mann, and Jürgen Cox. The perseus computational platform for comprehensive analysis of (prote)omics data. *Nature Methods*, 13(9):731–740, June 2016. ISSN 1548-7105. doi: 10.1038/nmeth.3901. URL http://dx.doi.org/10.1038/nmeth.3901.

[19] Zeeshan Hamid, Kip D. Zimmerman, Hector Guillen-Ahlers, Cun Li, Peter Nathanielsz, Laura A. Cox, and Michael Olivier. Assessment of label-free quantification and missing value imputation for proteomics in non-human primates. *BMC Genomics*, 23(1), July 2022. ISSN 1471-2164. doi: 10.1186/s12864-022-08723-1. URL http://dx.doi.org/10.1186/s12864-022-08723-1.

[20] Yoav Benjamini and Yosef Hochberg. Controlling the false discovery rate: A practical and powerful approach to multiple testing. *Journal of the Royal Statistical Society Series B: Statistical Methodology*, 57(1):289–300, January 1995. ISSN 1467-9868. doi: 10.1111/j.2517-6161.1995.tb02031.x. URL http://dx.doi.org/10.1111/j.2517-6161.1995.tb02031.x.

[21] Rebecca DerSimonian and Nan Laird. Meta-analysis in clinical trials. *Controlled Clinical Trials*, 7(3):177–188, September 1986. ISSN 0197-2456. doi: 10.1016/0197-2456(86)90046-2. URL http://dx.doi.org/10.1016/0197-2456(86)90046-2.

[22] Julian P. T. Higgins and Simon G. Thompson. Quantifying heterogeneity in a meta-analysis. *Statistics in Medicine*, 21(11):1539–1558, May 2002. ISSN 1097-0258. doi: 10.1002/sim.1186. URL http://dx.doi.org/10.1002/sim.1186.

[23] Julian P T Higgins, Simon G Thompson, Jonathan J Deeks, and Douglas G Altman. Measuring inconsistency in meta-analyses. *BMJ*, 327(7414):557–560, September 2003. ISSN 1468-5833. doi: 10.1136/bmj.327.7414.557. URL http://dx.doi.org/10.1136/bmj.327.7414.557.

[24] Christian Hennig. Cluster-wise assessment of cluster stability. *Computational Statistics & Data Analysis*, 52(1):258–271, September 2007. ISSN 0167-9473. doi: 10.1016/j.csda.2006.11.025. URL http://dx.doi.org/10.1016/j.csda.2006.11.025.

[25] Ge Tao, Agata K. Levay, Jacqueline D. Peacock, Danielle J. Huk, Sarah N. Both, Nicole H. Purcell, Jose R. Pinto, Maarten L. Galantowicz, Manuel Koch, Pamela A. Lucchesi, David E. Birk, and Joy Lincoln. Collagen xiv is important for growth and structural integrity of the myocardium. *Journal of Molecular and Cellular Cardiology*, 53(5):626–638, November 2012. ISSN 0022-2828. doi: 10.1016/j.yjmcc.2012.08.002. URL http://dx.doi.org/10.1016/j.yjmcc.2012.08.002.

[26] Carolina Gil-Cayuela, Miguel Rivera, Ana Ortega, Estefanía Tarazón, Juan Carlos Triviño, Francisca Lago, José Ramón González-Juanatey, Luis Almenar, Luis Martínez-Dolz, and Manuel Portolés. Rna sequencing analysis identifies new human collagen genes involved in cardiac remodeling. *Journal of the American College of Cardiology*, 65(12):1265–1267, March 2015. ISSN 0735-1097. doi: 10.1016/j.jacc.2015.01.029. URL http://dx.doi.org/10.1016/j.jacc.2015.01.029.

[27] Vivek Sarohi, Sanchari Chakraborty, and Trayambak Basak. Exploring the cardiac ecm during fibrosis: A new era with next-gen proteomics. *Frontiers in Molecular Biosciences*, 9, November 2022. ISSN 2296-889X. doi: 10.3389/fmolb.2022.1030226. URL http://dx.doi.org/10.3389/fmolb.2022.1030226.

[28] Ella G. Frolova, Nikolai Sopko, Lauren Blech, Zoran B. Popović, Jianbo Li, Amit Vasanji, Carla Drumm, Irene Krukovets, Mukesh K. Jain, Marc S. Penn, Edward F. Plow, and Olga I. Stenina. Thrombospondin-4 regulates fibrosis and remodeling of the myocardium in response to pressure overload. *The FASEB Journal*, 26(6):2363–2373, February 2012. ISSN 1530-6860. doi: 10.1096/fj.11-190728. URL http://dx.doi.org/10.1096/fj.11-190728.

[29] Mohammed Tanjimur Rahman, Santoshi Muppala, Jiahui Wu, Irene Krukovets, Dmitry Solovjev, Dmitriy Verbovetskiy, Chioma Obiako, Edward F. Plow, and Olga Stenina-Adognravi. Effects of thrombospondin-4 on pro-inflammatory phenotype differentiation and apoptosis in macrophages. *Cell Death & Disease*, 11(1), January 2020. ISSN 2041-4889. doi: 10.1038/s41419-020-2237-2. URL http://dx.doi.org/10.1038/s41419-020-2237-2.

[30] Matthias Dupont, Wilfried Mullens, and W. H. Wilson Tang. Impact of systemic venous congestion in heart failure. *Current Heart Failure Reports*, 8(4):233–241, August 2011. ISSN 1546-9549. doi: 10.1007/s11897-011-0071-7. URL http://dx.doi.org/10.1007/s11897-011-0071-7.

[31] Madhumita Paul and Omar Skalli. *Synemin*, pages 537–555. Elsevier, 2016. ISBN 9780128034705. doi: 10.1016/bs.mie.2015.08.005. URL http://dx.doi.org/10.1016/bs.mie.2015.08.005.

[32] B. Delia Johnson, Kevin E. Kip, Oscar C. Marroquin, Paul M Ridker, Sheryl F. Kelsey, Leslee J. Shaw, Carl J. Pepine, Barry Sharaf, C. Noel Bairey Merz, George Sopko, Marian B. Olson, and Steven E. Reis. Serum amyloid a as a predictor of coronary artery disease and cardiovascular outcome in women: The national heart, lung, and blood institute–sponsored women's ischemia syndrome evaluation (wise). *Circulation*, 109(6):726–732, February 2004. ISSN 1524-4539. doi: 10.1161/01.cir.0000115516.54550.b1. URL http://dx.doi.org/10.1161/01.CIR.0000115516.54550.B1.

[33] Paul M. Ridker, Nader Rifai, Lynda Rose, Julie E. Buring, and Nancy R. Cook. Comparison of c-reactive protein and low-density lipoprotein cholesterol levels in the prediction of first cardiovascular events. *New England Journal of Medicine*, 347(20):1557–1565, November 2002. ISSN 1533-4406. doi: 10.1056/nejmoa021993. URL http://dx.doi.org/10.1056/NEJMoa021993.

[34] Markus Ketteler, Philipp Bongartz, Ralf Westenfeld, Joachim Ernst Wildberger, Andreas Horst Mahnken, Roland Böhm, Thomas Metzger, Christoph Wanner, Willi Jahnen-Dechent, and Jürgen Floege. Association of low fetuin-a (ahsg) concentrations in serum with cardiovascular mortality in patients on dialysis: a cross-sectional study. *The Lancet*, 361(9360):827–833, March 2003. ISSN 0140-6736. doi: 10.1016/s0140-6736(03)12710-9. URL http://dx.doi.org/10.1016/s0140-6736(03)12710-9.

[35] Amelia C. Peterson, Jason D. Russell, Derek J. Bailey, Michael S. Westphall, and Joshua J. Coon. Parallel reaction monitoring for high resolution and high mass accuracy quantitative, targeted proteomics. *Molecular & Cellular Proteomics*, 11(11):1475–1488, November 2012. ISSN 1535-9476. doi: 10.1074/mcp.o112.020131. URL http://dx.doi.org/10.1074/mcp.O112.020131.

[36] Vinzenz Lange, Paola Picotti, Bruno Domon, and Ruedi Aebersold. Selected reaction monitoring for quantitative proteomics: a tutorial. *Molecular Systems Biology*, 4(1), October 2008. ISSN 1744-4292. doi: 10.1038/msb.2008.61. URL http://dx.doi.org/10.1038/msb.2008.61.

[37] Paola Picotti and Ruedi Aebersold. Selected reaction monitoring–based proteomics: workflows, potential, pitfalls and future directions. *Nature Methods*, 9(6):555–566, May 2012. ISSN 1548-7105. doi: 10.1038/nmeth.2015. URL http://dx.doi.org/10.1038/nmeth.2015.

[38] Ioannis Karakikes, Mohamed Ameen, Vittavat Termglinchan, and Joseph C. Wu. Human induced pluripotent stem cell–derived cardiomyocytes: Insights into molecular, cellular, and functional phenotypes. *Circulation Research*, 117(1):80–88, June 2015. ISSN 1524-4571. doi: 10.1161/circresaha.117.305365. URL http://dx.doi.org/10.1161/CIRCRESAHA.117.305365.

[39] Patrizia Dell'Era. Cardiac disease modeling using induced pluripotent stem cell-derived human cardiomyocytes. *World Journal of Stem Cells*, 7(2):329, 2015. ISSN 1948-0210. doi: 10.4252/wjsc.v7.i2.329. URL http://dx.doi.org/10.4252/wjsc.v7.i2.329.

[40] Daniel A. Richards, Mark J. Aronovitz, Timothy D. Calamaras, Kelly Tam, Gregory L. Martin, Peiwen Liu, Heather K. Bowditch, Phyllis Zhang, Gordon S. Huggins, and Robert M. Blanton. Distinct phenotypes induced by three degrees of transverse aortic constriction in mice. *Scientific Reports*, 9(1), April 2019. ISSN 2045-2322. doi: 10.1038/s41598-019-42209-7. URL http://dx.doi.org/10.1038/s41598-019-42209-7.

[41] Mohashin Pathan, Shivakumar Keerthikumar, Ching-Seng Ang, Lahiru Gangoda, Camelia Y.J. Quek, Nicholas A. Williamson, Dmitri Mouradov, Oliver M. Sieber, Richard J. Simpson, Agus Salim, Antony Bacic, Andrew F. Hill, David A. Stroud, Michael T. Ryan, Johnson I. Agbinya, John M. Mariadason, Antony W. Burgess, and Suresh Mathivanan. Funrich: An open access standalone functional enrichment and interaction network analysis tool. *PROTEOMICS*, 15(15):2597–2601, June 2015. ISSN 1615-9861. doi: 10.1002/pmic.201400515. URL http://dx.doi.org/10.1002/pmic.201400515.